Drone Flight Scheduling Under Uncertainty on Battery Duration and Air Temperature

Seon Jin Kim[a], Gino J. Lim[a,*], Jaeyoung Cho[b]

[a] *Department of Industrial Engineering, University of Houston, Houston, TX 77204, USA*
[b] *Department of Industrial Engineering, Lamar University, Beaumont, TX 77710, USA*

Abstract

Commercial drones are expected to be widely used in the near future. They are generally powered by batteries to fly aerial areas. Flying time performance is known to change depending on air temperature. Hence, this paper proposes a robust optimization approach to find the optimal flight schedule (i.e., the number of drones and flight paths) in the flight network considering uncertain battery duration. A regression model is first developed to estimate battery duration as a function of air temperature. Three flight duration uncertainty sets (polyhedral, box, and ellipsoidal) are explored based on the regression model, and the robust optimization model is solved for each of the three sets. A decision tool is developed to analyze performance of the sets, and to help a decision maker select an appropriate uncertainty set that is most appropriate for a specific application of interest. The tool considers both minimizing the total operating cost and minimizing the probability of not completing the scheduled flights. Numerical results are presented to illustrate the proposed method.

Keywords: Drone flight schedule, Uncertainty, Robust optimization, Battery capacity

1. Introduction

Unmanned aerial vehicles (UAVs), also known as drones, receive a tremendous amount of attention from civilian, commercial, and military sectors across the globe as means of monitoring situations and delivering demands. Examples include British Petroleum (BP)'s test on drones to monitor its pipelines and oil fields at Prudhoe Bay in Alaska (Nichols,

*Corresponding author
Email addresses: sonjin64@gmail.com (Seon Jin Kim), ginolim@uh.edu (Gino J. Lim), uncmac.rokag@gmail.com (Jaeyoung Cho)

2014; Benham, 2015); Amazon's preparation to use drones for package delivery (Stolaroff, 2014); and Nepal's use of drones to monitor areas damaged by the April 2015 earthquake (Daly, 2015). These applications suggest that drones can be flown at any time throughout the year and can be flown in harsh environments.

Batteries power drones' wing rotations. Colder temperatures greatly reduce drone battery performance (Leng et al., 2015), and this in turn reduces the drone flight time (Hsu, 2013). If there seems to be significant changes in temperature over a drone operating period in the same area and if the performance is affected by the temperature, concerns must be raised about the scheduling of drone flights to avoid potential failure of scheduled delivery. Different discharge curves of a lithium-ion battery under varying temperatures (from $-10°$C to $50°$C) are shown in Figure A in Appendix A.

The capacity (% rated) in Figure A represents the amount of energy that can be extracted from the battery under given surrounding temperatures against a nominal amount (100%) of the battery's energy. The figure shows that performance of the battery is reduced when the temperature is below $20°$C, and there is a 25% reduction in battery capacity at $-10°$C ($100\% \rightarrow 75\%$). Thus, if not accounted for during the planning stages of the drone flight, temperature-induced reductions in battery performance may result in drones failing to return to their launch sites and/or meet service demands. To compensate for the reduced flight time, drone flight planners must either increase the number of drones or employ higher-performance batteries to meet all planned demands in temperatures below $20°$C.

Changes in temperature are uncertain and the uncertainty in temperature change is mostly expressed as a range (Kunreuther et al., 2013). A range of temperature changes can be obtained using observed data. However, a comprehensive relation between temperature and battery capacity has not been well addressed in the literature (Rao et al., 2003; Lu et al., 2013). Many researchers have reported experimental data suggesting approximate relationships between the two, and some ranges of the battery capacity change have been provided corresponding to temperature changes. To identify optimal and feasible drone flight schedules for real-world applications, researchers must account for the uncertainties in temperature changes and battery capacity changes.

Hence, in this paper, we propose a robust optimization approach to addressing the uncer-

tainty in battery capacity changes corresponding to air temperature changes and identifying specific drone flight paths that cover all demands in uncertain environments. We also introduce the use of two measurements (cost ratio and probabilistic guarantee) to assess the performance of uncertainty sets. Although robust optimization does not need probabilistic distribution information, decision makers may require probabilistic guarantees to determine which uncertainty set is needed to minimize the probability of not completing the scheduled flights in reality (Li et al., 2012).

To solve this problem, we perform the work that follows the processes shown in Figure 1. First, we identify uncertain factors and its information, in which the factors are not stochastic and have no available distributional information, and identify the best method to solve this kind of problem. Second, we develop a mathematical formulation model to represent the features of a drone flight schedule that would accomplish the aim of this work. Third, given uncertainty sets, we derive the robust counterpart (deterministic expression) for each set. Scenarios (the ranges of battery capacity changes) are obtained by regression analysis using forecasted data and the experimental relation between temperature and battery capacity. Using the counterpart of the robust problem and scenarios, we obtain a robust solution (drone flight schedule) and the corresponding optimal value (total operating cost). Finally, we analyze the optimal values of the three sets using cost ratios and probabilistic guarantees of varying uncertain set sizes.

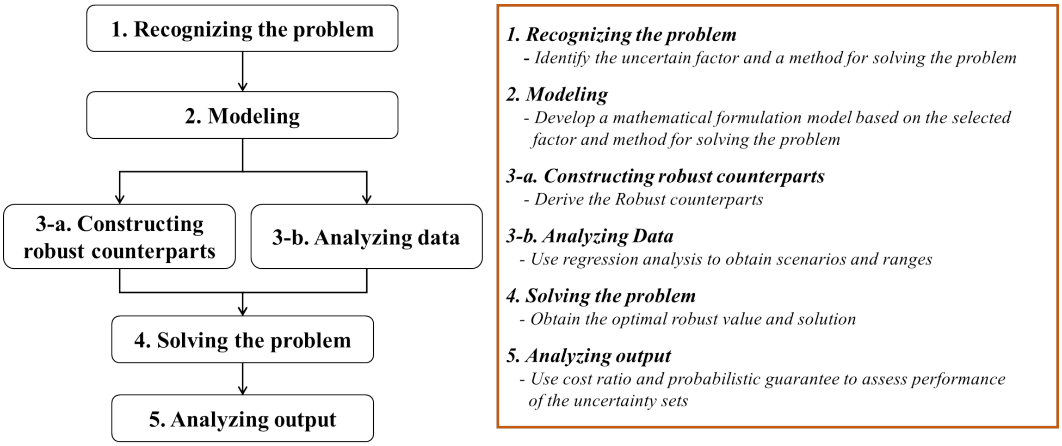

Fig. 1. Framework for solving the problem

This paper contributes to the existing body of literature as follows:

- To present a robust optimization approach (Bertsimas et al., 2011) to handle uncertain flight duration of a drone for a given flight path in a network environment.
- To provide decision makers with analysis tools to help select an appropriate model configuration under flight time duration uncertainty: (1) a cost ratio to show how much additional cost may incur when the schedule is developed considering uncertain flight durations, and (2) a probabilistic guarantee to evaluate a feasibility for a robust solution in a given configuration.
- To provide a simple approach to find the minimum flight time to guarantee feasibility of satisfying demands under uncertainty. A given minimum flight time may not be sufficient to complete a planned flight schedule due to a significant temperature change.

The rest of this paper is organized as follows. A literature review is presented in Section 2. Section 3 describes the problem in detail and presents the robust optimization model applied to find the solution, in which three robust counterparts are introduced. A method to find ranges of uncertain deviations is also described in Section 3. In Section 4, a case study is used to illustrate the effectiveness of the proposed model in practice, and an analysis of the results of the three sets, conducted using two performance measurements, is described. Finally, Section 5 includes a discussion of the highlights in this paper and the potential extension of this work.

2. Literature Review

There has been an increasing interest of using drones for commercial delivery services and for monitoring border lines, power lines, fires, soil erosion, volcanic activity, and security management (Kim and Lim, 2018; Kim et al., 2017; d'Oleire Oltmanns et al., 2012; McGonigle et al., 2008; Cho et al., 2015; Merino et al., 2005). Kim et al. (Kim and Lim, 2018) proposed a drone-aided border line surveillance method with a new battery charging system, which is a novel approach to extend the battery capacity during flights without considering flight environments. Lim et al. (Lim et al., 2016) and Deng et al. (Deng et al., 2014) proposed a method of using multiple drones to inspect power lines and assumed a fixed flight

time. d'Oleire-Oltmanns et al. (d'Oleire Oltmanns et al., 2012) presented a method of using drones to monitor soil erosion in Morocco and also specified a fixed flight time. Cho et al. (Cho et al., 2015) suggested drone-aided security operations in the oil and gas industry, in which the optimal flight schedule for drones being used for port facilities' surveillance was obtained with a fixed flight time. Torres-Sánchez et al. (Torres-Sánchez et al., 2013) and Bellvert et al. (Bellvert et al., 2014) demonstrated using drones for image acquisition to receive data in real time and to improve a data quality.

The vast majority of the literature have proposed the drone flight scheduling problem based on nominal (i.e., deterministic) flight times and speeds without considering flight environments. Others have taken external factors affecting flight times into consideration. For example, Kim et al. (Kim et al., 2017) considered both symmetric and asymmetric flight times to reflect real flight environments such as winds and obstacles, which can affect the flight time between two nodes. Al-Sabban et al. (Al-Sabban et al., 2013) presented Markov decision processes for planning drone flights under uncertain wind direction conditions, in which time-varying wind was considered. Langelaan et al. (Langelaan et al., 2011) described a method of estimating three-dimensional wind fields to figure out how the wind affects the drone flight times.

Although the effect of wind has been investigated by several researchers, the effect of air temperature on drone scheduling has not been well addressed. Therefore, this paper aims to develop an optimization approach to schedule drone flights with temperature-induced reductions of battery performance.

3. Problem Description and Model Formulation

3.1. Problem Description

This paper presents the robust optimization approach to address the impact of changes in air temperature on drone battery capacity. Significant changes in air temperature during drone operation over an area can impact a planned flight schedule (the number of drones and specific flight paths of each drone) due to changes in battery capacity associated with air temperature. Therefore, the effects of changes in air temperature on battery capacity

need to be considered in the planning phase. The aim of this work is to find optimal drone flight schedules that minimize operating costs while satisfying given demands.

This work considers multiple depots as initial launch points, and each demand is met by one drone that returns to the initial launch point. Once the drones return to the initial launch point, they are re-utilized for the following schedule after battery replacement. The operating cost of a drone is incurred when the drone is utilized, and the amount of the cost is fixed as a constant value regardless of the drone's flight distance. The operating cost often includes expenses associated with control center operation, drone maintenance, personnel, and drone's depreciation cost. As per their specifications, most commercial drones have to return to their initial launch point within 1 hour. Hence, in this work, drone flight schedules are on an hourly basis. The battery is assumed to be a lithium battery, whose performance is easily affected by surrounding air temperature (Lu et al., 2013; Rao et al., 2003). The use of isolated capsules and other techniques to reduce the influence of air temperature on battery capacity are beyond of the scope of this paper. The maximum possible drone flight distance is determined by battery capacity and is proportional to the maximum possible drone flight time ($1\ min = 1\ mile$). Note that flight times (or distance) between two nodes are given input to the optimization model, and it considers an external force such as wind changes.

We use the following notation to develop the drone scheduling model (DSM).

Indices

I	Set of customer nodes ($i, j \in I$)
C	Set of center (depot) nodes ($c \in C$)
K	Set of drones ($k \in K$)

Parameters

p_k	Operating cost of drone k
d_{ci}, d_{ij}	Flight distance (time) between a center (c) and a node (i) or between nodes (i, j)
t_k	Maximum flight duration of drone k

Decision Variables Our aim is to determine optimal drone flight paths while minimizing the total operating cost (i.e., the total number of drones). Accordingly, we define de-

cision variables as:

x_{ijk} 1 if drone k flies from node i to j, 0 otherwise

h_k 1 if drone k is utilized to serve, 0 otherwise

μ_i Sequence of visiting node i in a path

3.2. Formulation of the DSM

The deterministic formulation of the DSM is expressed below:

$$\text{Minimize} \quad z = \sum_{k \in K} p_k \times h_k \tag{1}$$

$$\text{Subject to:} \quad \sum_{i \in I \cup C} \sum_{k \in K} x_{ijk} = 1, \qquad \forall j \in I \tag{2}$$

$$\sum_{j \in I \cup C} \sum_{k \in K} x_{ijk} = 1, \qquad \forall i \in I \tag{3}$$

$$x_{iik} = 0, \qquad \forall i \in I \cup C,\ k \in K \tag{4}$$

$$\sum_{j \in I} x_{cjk} - \sum_{i \in I} x_{ick} = 0, \qquad \forall c \in C,\ k \in K \tag{5}$$

$$\sum_{c \in C} \sum_{j \in I} x_{cjk} = h_k, \qquad \forall k \in K \tag{6}$$

$$\sum_{i \in I} \sum_{c \in C} x_{ick} = h_k, \qquad \forall k \in K \tag{7}$$

$$\sum_{i \in I \cup C} x_{iuk} - \sum_{j \in I \cup C} x_{ujk} = 0, \qquad \forall u \in I,\ k \in K \tag{8}$$

$$\sum_{i \in I \cup C} \sum_{j \in I \cup C} d_{ij} \times x_{ijk} \leq\ t_k, \qquad \forall k \in K, t_k \in U_T \tag{9}$$

$$\mu_i - \mu_j + n \sum_{k} x_{ijk} \leq\ n - 1, \qquad \forall i, j \in I \tag{10}$$

$$x_{ijk}, h_k \in \{0, 1\}, \mu_i \geq 0, n = |I|.$$

The objective function (1) minimizes the sum of the operating cost of the drones, which helps to minimize the number of drones. Constraints (2) and (3) ensure that each customer node is served only once. Constraint (4) is set to prevent a drone from revisiting the same customer or center, and Constraint (5) ensures a drone to return to where it departed from. Constraints (6) and (7) describe the utilization condition of the drones. Constraint (8) is

used to conserve the flow of drone flight at customer nodes as well as centers. The maximum possible flight time of drone k is represented in Constraint (9), in which parameter t_k is an uncertain value belonging to a bounded set U_T. The Miller-Tucker-Zemlin formulation (Miller et al., 1960; Öncan et al., 2009) is used in Constraint (10) to eliminate sub-tours.

3.3. Uncertainty Sets

We consider closed (bounded) uncertainty sets which are constructed as deviations from an expected value (t_k^0) of battery capacity (t_k) in Constraint (9). This means that the battery capacity can vary within a given set of uncertainty associated with temperature changes. The deviations are fixed and identified by a number of scenario vectors (t_k^s), which are allowed to have negative deviation values. For a given number of scenario vectors s ($\in S$), the general uncertainty set (U_T) is a linear combination of scenario vectors with weight $y_s \in Y$:

$$U_T = \{t_k \mid t_k^0 + \sum_{s=1}^{\Omega} y_s t_k^s, \quad \forall y_s \in Y\}$$

Hence, Constraint (9) can be written as follows:

$$\sum_i \sum_j x_{ijk}\ d_{ij} - t_k^0 \leq \sum_{s=1}^{\Omega} y_s t_k^s. \tag{11}$$

To enforce that the inequality holds for all y_s ($\in Y$), it suffices to impose it for

$$min_{y_s \in Y} \sum_{s=1}^{\Omega} y_s t_k^s$$

One of the challenges of applying the robust optimization approach to solve a problem is yo find an appropriate uncertainty set describing the problem well (i.e., choosing a proper uncertainty set). If the selected set of uncertainty is too large, then it can yield robust solutions that are too conservative to ensure feasibility under any circumstances. Consequently, it may result in an unnecessarily higher cost. Hence, the cost ratio and the probabilistic guarantee are suggested to choose the best uncertainty set in Section 4.4.

For uncertainty set (Y), we examine three uncertainty sets proposed by Bertsimas et al. (2011):

1. Polyhedral set: $Y_1 = \{y \mid y_s \geq 0, \quad \sum_{s=1}^{\Omega} y_s \leq 1\} : U_{T_1}$

2. Box set: $Y_2 = \{y \mid |y_s| \leq 1, \quad s = 1, ...\Omega\} : U_{T_2}$

3. Ellipsoid set: $Y_3 = \{y \mid \sum_{s=1}^{\Omega} y_s^2 \leq 1\} : U_{T_3}$

The box set will be appropriate if uncertain changes in battery capacity are assumed to remain in a given range of two extreme values. The ellipsoid set should be used the pattern of deviations from a nominal battery capacity can be captured by quadratic surfaces based on historical data and statistic tests (Gorissen et al., 2015). The polyhedral uncertainty set is a special case of ellipsoidal uncertainty (Bertsimas et al., 2011)

The robust counterpart, a deterministic equivalent value corresponding to each uncertainty set, is needed to get robust solutions. The robust counterparts of the three uncertainty sets are derived as follows:

Proposition 1. *Under the uncertainty set U_{T_1}, the robust counterpart is equivalent to the following constraint (i.e., by replacing Constraint (9) with the following constraint):*

$$\sum_i \sum_j x_{ijk} d_{ij} - t_k^0 \leq \min\{\min_{s \in S} t_k^s, 0\}, \quad \forall k \in K \tag{12}$$

Proof. See Appendix B for details. □

Proposition 2. *Under the uncertainty set U_{T_2}, the robust counterpart is equivalent to the following constraint (i.e., by replacing Constraint (9) with the following constraint):*

$$\sum_i \sum_j x_{ijk} d_{ij} - t_k^0 \leq -\sum_{s=1}^{\Omega} |t_k^s|, \quad \forall k \in K \tag{13}$$

Proof. See Appendix C for details. □

Proposition 3. *Under the uncertainty set U_{T_3}, the robust counterpart is equivalent to the following constraint (i.e., by replacing Constraint (9) with the following constraint):*

$$\sum_i \sum_j x_{ijk} d_{ij} - t_k^0 \leq -\sqrt{(t_k^1)^2 + ... + (t_k^{\Omega})^2}, \quad \forall k \in K \tag{14}$$

Proof. See Appendix D for details. □

3.4. Using Regression Analysis to Find t_k^s

This section describes the data analysis required to obtain scenarios and intervals (t_k^s) for the models introduced in Section 3.3. Battery capacity changes corresponding to temperature changes are not known exactly or comprehensively. As a result, we use forecasted weather data and experimental battery discharge rates (Figure A) to estimate the relation. The framework for finding t_k^s is shown in Figure 2.

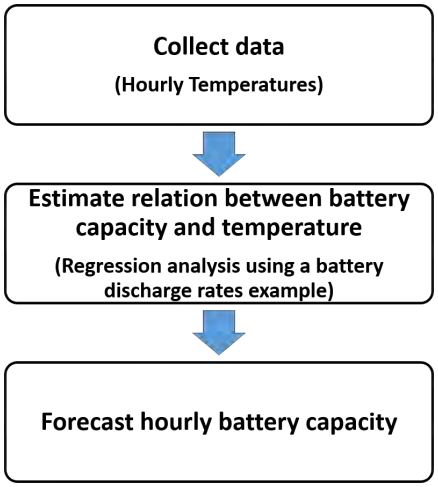

Fig. 2. Framework for finding t_k^s

First, both historical and forecast temperature data for a specified area in which the drones will operate are collected. On the basis of the assumptions listed in Section 3.1, low hourly temperature data are needed to obtain the drones' hourly flight plans. Using the two sets of data, we can estimate the future hourly temperature over the area. The initial estimated hourly temperatures are adjusted for the drones' flight altitude (Kattel et al., 2013; FAA, 2016).

Second, we obtain a model of the relation between battery capacity changes and air temperature changes (i.e., the adjusted hourly temperature changes). To estimate the relation between the two, we use the regression analysis method, in which the independent variable is temperature and the dependent variable is rated battery capacity. The method is illustrated with an example of an existing battery discharge rate.

Last, we use the estimated relation model to convert the adjusted hourly temperatures into hourly rated battery capacity. The converted hourly capacity values are then used to generate scenarios (deviations of nominal flight time) in the next section.

4. Numerical Experiments

This section consists of four parts. First, we describe a case study and historical data to estimate an hourly air temperature change over time. The regression model is then developed using the data, and bounds of flight times are obtained accordingly. Second, we test the proposed robust models in the area corresponding to the historical data. Third, we propose a method to obtain feasible solutions when the original model is infeasible due to an insufficient minimum flight time assumption to complete a planned flight in the model. Outputs from the three sets are discussed in terms of cost ratio and probability guarantee, and the best uncertainty set is identified in the last part. All models are implemented in GAMS (GAMS Development, 2015) and solved by CPLEX 12.6.2 (IBM, 2015), and all experiments are performed on a server running RedHat Linux 64-bit with an Intel Xeon processor and 16GB of RAM.

4.1. Case Study

The selected case study includes 12 checkpoints and 2 drone centers (initial launch points) located just north of Austin, TX. The mission of the drones is to patrol all 12 checkpoints every hour from 7 $a.m.$ to 6 $p.m.$ All drones are the same type, and the drones' nominal flight time and distance are 35 minutes and 35 miles (not maximum flight range), respectively. The drones' flight altitude is 400 feet above, and each drone's per-flight operating cost is \$35.

The collected raw data represents hourly temperature data in the selected area on January 17, 2016 (NOAA, 2015). Detailed temperature data including the minimum temperature per hour are given in Figure E. The lapse rate is applied to obtain the adjusted temperature (Kattel et al., 2013); adjusted temperature = raw minimum temperature - temperature decrease with altitude 400 feet. The raw temperatures and the corresponding adjusted temperatures are shown in Table 1.

Table 1

Hourly temperature changes north of Austin, TX, on January 17, 2016, and corresponding battery capacity changes

	Time											
	7 a.m.	8	9	10	11	12 p.m.	1	2	3	4	5	6 p.m.
Raw Temp.(°C)	5.1	5.0	6.8	9.7	11.3	14.8	17.6	17.5	17.4	18.4	17.8	16.2
Adjusted Temp.(°C)	4.55	4.45	6.25	9.15	10.75	14.25	17.05	16.95	16.85	17.85	17.25	15.65
Est. Battery Cap (%)	92	92	93	95	97	99	100	100	100	100	100	99
Deviation (%)	-8	-8	-7	-5	-3	-1	0	0	0	0	0	-1

Next, using the data shown in Figure A, we conduct regression analysis to obtain a model of the relation between temperature and battery capacity. The resulting regression model is

$$Capacity = 0.8814 + 0.0091 \times Temperature - 0.0001 \times Temperature^2 \tag{15}$$

The *R-squared* value of the model is 0.9756 and the p-values for all parameters are less than 0.006. Because there does not exist a relation model between the temperature and the battery capacity change in the literature, the regression model (15) is used to estimate the temperature-induced reduction (i.e., deviation) in battery performance as shown in Table 1. For example, the maximum deviation of battery capacity between 7 and 8 $a.m.$ is estimated to be 8% (= 100% - 92%).

4.2. Numerical Results

Using the results described in Section 4.1, we solved the DSM for 7 random scenarios (see Table 2).

Table 2

Number of required drones at each time for three uncertainty sets

	Time												
	7 a.m.	8	9	10	11	12 p.m.	1	2	3	4	5	6 p.m.	Total
Set 1:													
No. of drones	7	7	7	6	6	6	5	5	5	5	5	6	7
Cost ($)	245	245	245	210	210	210	175	175	175	175	175	210	2,450
Set 2:													
No. of drones	INF	INF	INF	INF	9	6	5	5	5	5	5	6	N/A
Cost ($)	N/A	N/A	N/A	N/A	315	210	175	175	175	175	175	210	N/A
Set 3:													
No. of drones	9	9	9	7	6	6	5	5	5	5	5	6	9
Cost ($)	315	315	315	245	210	210	175	175	175	175	175	210	2,695
Deterministic:													
No. of drones	5	5	5	5	5	5	5	5	5	5	5	5	5
Cost ($)	175	175	175	175	175	175	175	175	175	175	175	175	2,100

INF : infeasible instance, N/A : an optimal value could not be found.

Compared with drone operation under the deterministic assumption, drone operation under each uncertainty set requires more drones and higher operating costs. Under Uncertainty Set 1, seven drones are needed, and the resulting daily cost of drone operation is $2,450. At least some of the 7 drones are assigned to patrol 12 checkpoints every hour. Under Uncertainty Set 2, given the nominal flight time of 35 minutes, drones operating between 7 $a.m.$ and 10 $a.m.$ cannot return to a center. They require a nominal flight time of longer than 35 minutes to complete the patrol missions. Compared with Uncertainty Set 1, Uncertainty Set 3 results in more drones and greater operating costs. Therefore, Uncertainty Set 2 (i.e., a simple bound set) appears to be most conservative among the three uncertainty sets for the test problems used for this section. It turns out that the solution under Uncertainty Set 2 is feasible for any demand realizations for sets 1, 2 and 3, whereas the solution under Uncertainty Set 1 is only feasible for the assumed uncertainty set (i.e., polyhedral set).

The drones' hourly flight paths under Uncertainty Set 1 are shown in Figure 3. Detailed flight paths under Uncertainty Set 3 are given in Figure F.

As shown in Table 2, 7 drones are required to conduct the mission from 7 to 9 $a.m.$, but after these times, 5 or 6 drones are sufficient. Although the numbers of required drones are the same, the flight routes may be different. For example, the numbers of drones from 10

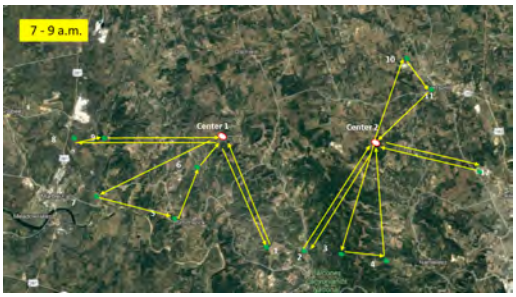

(a) From 7 a.m. to 9 a.m.

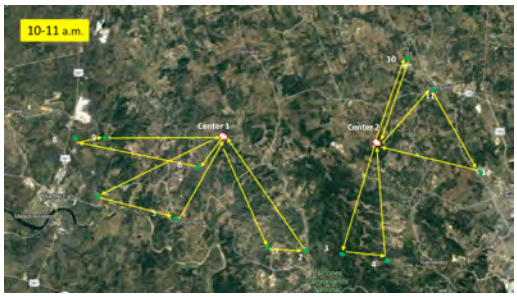

(b) From 10 a.m. to 11 a.m.

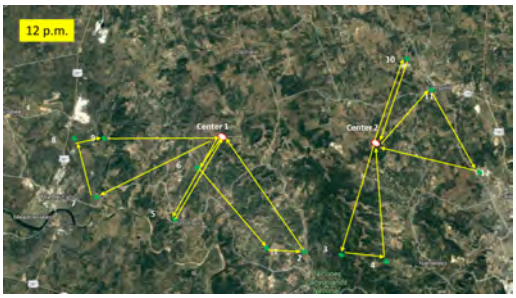

(c) At 12 p.m.

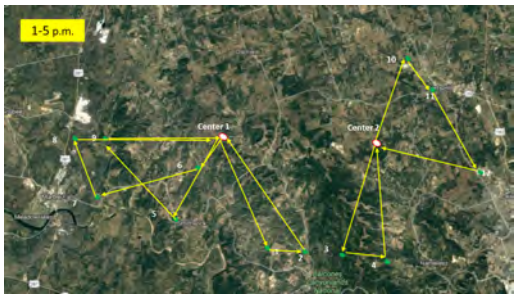

(d) From 1 p.m. to 5 p.m.

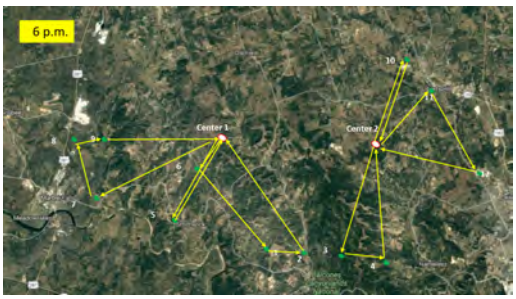

(e) At 6 p.m.

Fig. 3. Hourly flight paths under Uncertainty Set 1

a.m. to 12 *p.m.* and at 6 *p.m.* are the same (6 drones), but the detailed flight paths taken at 12 *p.m.* (Figure 3(c)) and 6 *p.m.* (Figure 3(e)) are different from the paths taken 10 to 11 *a.m.* (Figure 3(b)). We can choose one of the two different routes to patrol the checkpoints during the above times.

The numerical results showed that the optimization approach considering uncertain battery durations provided more conservative solutions than the nominal counterpart to ensure feasibility under any realizations of the temperature changes and the corresponding battery capacity reductions, at a higher costs. In Figure 4, we compared the optimal solution of

deterministic model with the one from the robust optimization model under Uncertainty Set 1, which is the least conservative among three sets. In practice, it might be impossible to patrol 12 checkpoints from 7 *a.m.* to 12 *p.m.* if the optimal deterministic solution is used (only five drones). As the amount of the temperature-induced reduction in battery capacity increases, the failure rate of returning to an initial depot increases under deterministic assumption. If we schedule the drone flights based on the deterministic assumption, three out of five drones may fail to return to its initial depot under the reduction scenarios ranging from 3% to 8%.

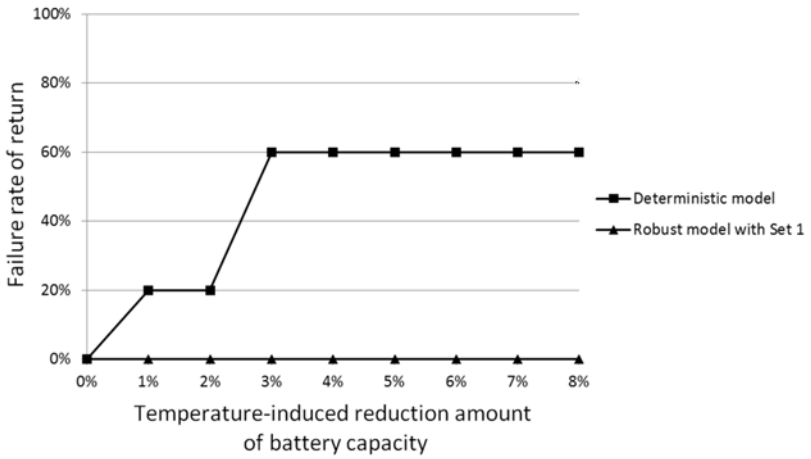

Fig. 4. Robustness of the proposed method compared with deterministic method

4.3. Recovery of Feasible Solutions

The infeasible cases (INF) in Table 2 are due to the violation in Constraint (13), in which a drone's projected total flight distance exceeded its maximum flight time (distance). One way to overcome this issue to equip the drones with enhanced batteries, which will enable a longer flight time. Furthermore, using a conservative estimate on the nominal total flight time to complete a tour in the scheduling model can help avoid the infeasibility issue. To estimate the minimum required nominal flight time to ensure feasibility, we use the longest round-trip flight distance between a center and a node (checkpoint). Specifically, we obtain the minimum required nominal flight time (t_k^0) satisfying Constraint (13) under Uncertainty

Set 2 using the equation below:

$$\begin{aligned} &\text{Objective} && min \quad t_k^0 \\ &\text{Subject to:} && Max(d_{ci} + d_{ic}) + \sum_{s=1}^{\Omega} |t_k^s| \leq t_k^0, \qquad \forall c \in C, i \in I \end{aligned} \tag{16}$$

where d_{ci} is a flight distance from a center to a node, and d_{ic} is a flight distance from a node to a center. The second term in Constraint (16) is the robust counterpart under Uncertainty Set 2, in which the deviation of capacity also increases proportionally, corresponding to the nominal flight time of enhanced batteries (i.e., the value of deviations of battery capacity is determined by the estimated battery capacity reduction rate in Section 4.1). For the case study, the minimum nominal value under Uncertainty Set 2 is 47.25 minutes. The number of required drones with high-performance batteries and a nominal flight time of 47.25 minutes are shown in Table 3.

Table 3

Number of required drones using high-performance batteries (nominal flight time, 47.25 minutes)

	Time												
	7 a.m.	8	9	10	11	12 p.m.	1	2	3	4	5	6 p.m.	Total
Set 1	3	3	3	3	3	3	3	3	3	3	3	3	3
Set 2	6	6	5	4	3	3	3	3	3	3	3	3	6
Set 3	4	4	3	3	3	3	3	3	3	3	3	3	4
Deterministic	3	3	3	3	3	3	3	3	3	3	3	3	3

Note: All data are no. of drones.

4.4. Uncertainty Sets and Performance Measurements

Two measurements (cost ratio and probabilistic guarantee) are introduced to assess performance of each of the three uncertainty sets. First, the cost ratio is calculated as $\frac{z_r - z_d}{z_d}$ in which z_r is the optimal objective function value of a robust optimization model and z_d is the optimal objective function value of the deterministic problem. This ratio illustrates how much extra cost will be incurred when adopting the robust approach over the deterministic optimization model. As a result, the schedule will be more robust against the failure to safe return of drones which can immediately cause unmet demand.

Table 4

Cost ratios under a nominal flight time of 35 minutes

	Time												
Set	7 a.m.	8	9	10	11	12 p.m.	1	2	3	4	5	6 p.m.	Total
1	0.4	0.4	0.4	0.2	0.2	0.2	0	0	0	0	0	0.2	0.17
2	*N/A*	*N/A*	*N/A*	*N/A*	0.8	0.2	0	0	0	0	0	0.2	*N/A*
3	0.8	0.8	0.8	0.4	0.2	0.2	0	0	0	0	0	0.2	0.28

Note: N/A indicates that a cost ratio could not be found due to infeasible instance.

Table 5

Cost ratios under a nominal flight time of 47.25 minutes

	Time												
Set	7 a.m.	8	9	10	11	12 p.m.	1	2	3	4	5	6 p.m.	Total
1	0	0	0	0	0	0	0	0	0	0	0	0	0
2	1	1	0.67	0.33	0	0	0	0	0	0	0	0	0.25
3	0.33	0	0	0	0	0	0	0	0	0	0	0	0.03

The cost ratios are calculated as shown in tables 4 and 5. For example, the cost ratio at 7 *a.m.* under Set 1 in Table 4 is 0.4. This ratio means that operating drones under battery duration uncertain, modeled based on Uncertainty Set 1, will cost 40% more than that of the deterministic assumption. This is a direct result of adding 2 more drones for an early morning schedule when there are fluctuations in air temperature (see Table 2). However, the ratios remain at 0 during 1 *p.m.* and 5 *p.m.* because no significant air temperature fluctuations were forecasted for these time period. The column *Total* on Set 1 shows the ratio of 0.17. Hence, Uncertainty Set 1 will incur an additional 17% cost (i.e., \$2,100 $\rightarrow$ \$2,450, 0.17= $\frac{2{,}450-2{,}100}{2{,}100}$) compared with the total operating cost under the deterministic assumption. Cost analysis of other sets can be explained similarly. Note that, under Set 2 as shown in Table 2, no feasible solutions were found between 7 and 10 *a.m.* so that the cost ratios could not be determined for these infeasible instances and they are labeled as N/A.

As mentioned in Section 4.3, the infeasible instances are due to insufficient battery duration to complete a task under an assumed uncertainty set. To ensure flight time feasibility, we obtained the minimum nominal flight time (47.25 minutes) using the method introduced in Section 4.3. In Table 5, the cost ratio at 7 *a.m.* under Set 2 is 1 (100%). It means that the number of required drones under Uncertainty Set 2 is twice as many drones as under the

deterministic assumption (see Table 3).

The two tables showed that the robust optimization approach requires a higher operating cost to deal with uncertainty in battery capacity than the deterministic approach does. In the case in which the battery with a nominal flight time of 35 minutes is used (Table 4), the additional amounts of cost are 17% and 28% under Uncertainty Sets 1 and 3, respectively. Thus, the ellipsoid uncertainty set (Set 3) is more conservative than the polyhedral set (Set 1). In all feasible cases in which the battery with a nominal flight time of 47.25 minutes is used (Table 5), the box uncertainty set (Set 2) is more conservative than the ellipsoid set (Set 3).

Second, the probabilistic guarantee requires that the optimal solution of the robust problem with an uncertain set must satisfy the deterministic constraint (original constraint) with a probability of at least the probabilistic guarantee value (Ben-Tal and Nemirovski, 2000; Bertsimas and Sim, 2004). According to Ben-Tal et al. (Ben-Tal and Nemirovski, 2000) and Bertsimas et al. (Bertsimas and Sim, 2004), the probability bounds for three uncertainty sets are given as follows:

1. Polyhedral set: $1-e^{-\frac{\Gamma^2}{(2|J_i|)}}$, where Γ is the size of the polyhedron and $|J_i|$ is the number of uncertain parameters in the i-th constraint.

2. Box set: $1-e^{-\frac{\Delta^2}{2}}$, where Δ is the size of the box.

3. Ellipsoid set: $1-e^{-\frac{\Phi^2}{2}}$, where Φ is the radius of the ellipsoid.

In the polyhedral uncertainty set, the number of uncertain parameters is 1 ($|J_i|$=1). Therefore, the probability bound of the polyhedral set is the same as the bound of the ellipsoid set if the three sets have the same size ($e^{-\frac{\Gamma^2}{(2|J_i|)}} = e^{-\frac{\Delta^2}{2}} = e^{-\frac{\Phi^2}{2}}$ if $\Gamma = \Delta = \Phi$). Therefore, the values of the probability of satisfaction under Sets 1, 2, and 3 are the same, especially in this example.

Figure 5 shows a comparison of the probability of satisfaction with the size of Uncertainty Set 1 when a battery with a nominal flight time of 35 minutes used. First, the probability of satisfaction also monotonically increases as the set size increases. Second, the cost ratio remains flat at 0.117 until the set size reaches 0.7 and then shows an increasing pattern until

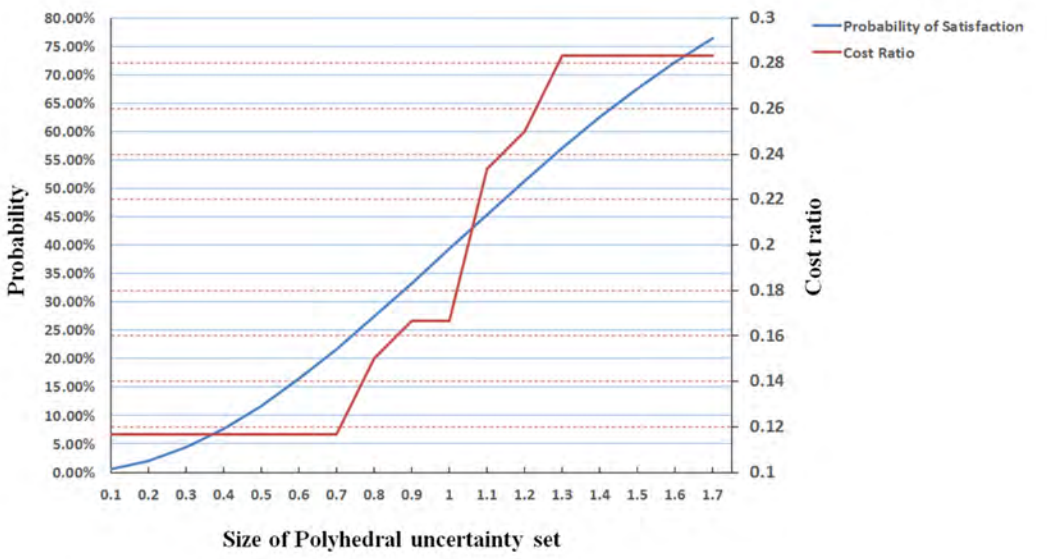

Fig. 5. Probability of satisfaction and cost ratio as a function of size of polyhedral uncertainty set (Uncertainty Set 1).

1.3. After that, it reaches a stationary state. Compared with Set 2 and Set 3, Set 1 (the polyhedral uncertainty set) has lower cost but the same probability of satisfaction

As one can see from these two measurements, there is a trade-off between the level of satisfaction (or robustness) and the associated cost. As the probability of satisfaction increases, the corresponding cost tends to increase. Decision makers can use this trade-off to find an appropriate uncertainty set size accomplishing a targeted satisfaction probability within a budget limit.

5. Conclusion

This paper introduced a robust optimization approach to the drone-scheduling problem to address the uncertainty of drone battery capacity caused by air temperature changes. We have explored three different uncertainty sets to describe the uncertainty of the battery capacity changes in the robust optimization model to find an solution (number of drones and their paths) and its corresponding objective value (minimum operating cost).

A regression model was developed to estimate the temperature-induced reduction (i.e., deviation) in battery performance. The proposed robust optimization model was then tested

using a case study. The results showed that the robust optimization approach should be used rather than the traditional deterministic optimization model in order to minimize the failure rate of drones to return to an initial depot. The box uncertainty set (Set 2) worked well for any demand realizations that were tested under sets 1, 2 and 3. Hence, using the box uncertainty set may be appropriate if one wants to ensure the return of drones to the depot in any realizations of battery capacity change. However, the polydehral set (Set 1) outperformed the other sets in terms of the cost ratio and the probability of satisfaction by incurring a lower cost for the same satisfaction level in all cases studied in this paper.

An extension of this work may include a study of real-time rescheduling based on real-time battery capacity reduction, in which the service priority of remaining demands can be considered. For example, an alternative flight path can be developed to minimize unmet demands if the remaining battery capacity falls below a threshold value due to temperature changes.

Appendix A

Discharge curves for a lithium-ion battery at different temperatures

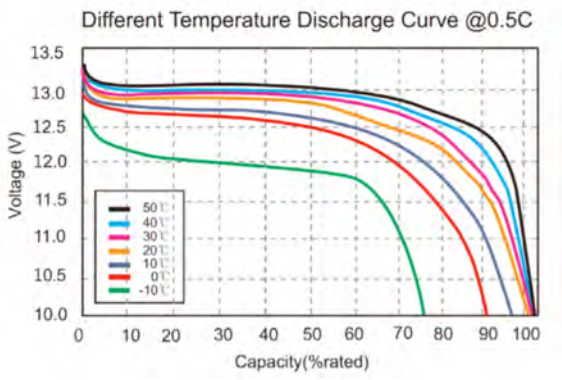

Fig. A. Discharge curves for a lithium-ion battery at different temperatures (Tech, 2016)

Appendix B

Proof of Proposition 1

Using the definition of the uncertainty set, $Y_1 = \{y \mid y_s \geq 0, \quad \sum_{s=1}^{\Omega} y_s \leq 1\}$, we obtain the primal LP and its dual as follows:

	$< Primal >$	$< Dual >$
Objective	$min \quad \sum_{s=1}^{\Omega} y_s t_k^s$	$max \quad -\omega$
Subject to:	$\sum_{s=1}^{\Omega} y_s \leq 1,$	$-\omega \leq t_k^s, \quad s = 1, ...\Omega$
	$y_s \geq 0$	$\omega \geq 0$

From the weak duality theorem (Bazaraa et al., 2011), the condition

$$\sum_i \sum_j x_{ijk}\ d_{ij} - t_k^0 \leq \sum_{s=1}^{\Omega} y_s t_k^s$$

is equivalent to

$$\sum_i \sum_j x_{ijk}\ d_{ij} - t_k^0 \leq -\omega$$

for some dual feasible ω. The above means that

$$\sum_i \sum_j x_{ijk}\ d_{ij} - t_k^0 \leq 0 \quad \text{and} \quad \sum_i \sum_j x_{ijk}\ d_{ij} - t_k^0 \leq t_k^s$$

Therefore, we obtain Constraint (12).

Appendix C

Proof of Proposition 2

Using the definition of the uncertainty set, $Y_2 = \{y \mid |y_s| \leq 1, \quad s = 1, ...\Omega\}$, we obtain the primal LP and its dual as follows:

	$< Primal >$	$< Dual >$
Objective	$min \quad \sum_{s=1}^{\Omega} y_s t_k^s$	$max \quad \mathbf{-1}^T(\omega_1 + \omega_2)$
Subject to:	$y_s \leq \mathbf{1},$	$-\omega_1 + \omega_2 = t_k^s, \quad s = 1, ...\Omega$
	$y_s \geq \mathbf{-1}$	$\omega_1, \omega_2 \geq 0$

where $\mathbf{1}$ is a column vector ($\Omega \times 1$) with all entries 1.

We can consider two cases for all scenarios: $t_k^s > 0$ and $t_k^s \leq 0$. In the case of $t_k^s > 0$, the objective function value of dual problem is $-t_k^s$ whereas the value of the objective function of dual problem is t_k^s in the case of $t_k^s \leq 0$. Therefore, from the weak duality theory (Bazaraa et al., 2011), we obtain the Constraint (13).

Appendix D

Proof of Proposition 3

Using the definition of the uncertainty set, $Y_3 = \{y \mid \sum_{s=1}^{\Omega} y_s^2 \leq 1\}$, we obtain the primal LP as follows:

$$< Primal >$$

$$\text{Objective} \qquad min \quad \sum_{s=1}^{\Omega} y_s t_k^s$$

$$\text{Subject to:} \qquad \sum_{s=1}^{\Omega} y_s^2 - 1 \leq 0$$

The feasible region of the primal problem is bounded. Hence, a global minimum solution must exist. From the Karush-Kuhn-Tucker (KKT) optimality necessary conditions (Gordon and Tibshirani, 2012), we obtain the Constraint (14).

Note that the feasible region is bounded ($\sum_{s=1}^{\Omega} y_s^2 \leq 1$), so a global minimum must exist. First, the Lagrangian function is constructed using the constant μ:

$$L(y, \mu) = y_1 t_k^1 + y_2 t_k^2 + \cdots + y_\Omega t_k^\Omega + \mu(y_1^2 + y_1^2 + \cdots + y_\Omega^2 - 1)$$

The first condition of KKT optimality ($f'(y_s^\star) + \mu^\star g; (y_s^\star) = 0$) is satisfied:

$$\frac{dL(y,\mu)}{dy_s} = t_k^s + 2\mu y_s = 0, \quad \frac{dL(y,\mu)}{d\mu} = y_1^2 + y_1^2 + \cdots + y_\Omega^2 - 1 = 0$$

$$Hence, \quad y_s^\star = -\frac{t_k^s}{\sqrt{(t_k^1)^2 + (t_k^2)^2 + \cdots + (t_k^\Omega)^2}} \quad and \quad \mu^\star = \frac{\sqrt{(t_k^1)^2 + (t_k^2)^2 + \cdots + (t_k^\Omega)^2}}{2}$$

The remaining three conditions are also satisfied:

$$g'(y_s^\star) \leq 0, \quad \mu^\star \geq 0, \quad and \quad \mu^\star g'(y_s^\star) = 0$$

with the values of $y_s^\star$ and $\mu^\star$

Appendix E

Raw hourly data in Austin, TX

23907	20150117	0800	20150117	0200	2.423	-98.08	30.62	7.3	7.5	8.1	7.2	0.0
23907	20150117	0900	20150117	0300	2.423	-98.08	30.62	6.7	6.8	7.4	6.4	0.0
23907	20150117	1000	20150117	0400	2.423	-98.08	30.62	6.6	6.5	6.7	6.1	0.0
23907	20150117	1100	20150117	0500	2.423	-98.08	30.62	5.9	5.9	6.6	5.3	0.0
23907	20150117	1200	20150117	0600	2.423	-98.08	30.62	5.3	5.5	5.9	5.3	0.0
23907	20150117	1300	20150117	0700	2.423	-98.08	30.62	5.2	5.3	5.6	5.1	0.0
23907	20150117	1400	20150117	0800	2.423	-98.08	30.62	6.8	5.7	6.8	5.0	0.0
23907	20150117	1500	20150117	0900	2.423	-98.08	30.62	9.7	8.4	9.8	6.8	0.0
23907	20150117	1600	20150117	1000	2.423	-98.08	30.62	11.3	10.6	11.3	9.7	0.0
23907	20150117	1700	20150117	1100	2.423	-98.08	30.62	14.8	12.9	14.8	11.3	0.0
23907	20150117	1800	20150117	1200	2.423	-98.08	30.62	17.5	16.1	17.6	14.8	0.0
23907	20150117	1900	20150117	1300	2.423	-98.08	30.62	18.6	18.6	19.3	17.6	0.0
23907	20150117	2000	20150117	1400	2.423	-98.08	30.62	17.5	18.3	19.5	17.5	0.0
23907	20150117	2100	20150117	1500	2.423	-98.08	30.62	18.7	18.0	18.7	17.4	0.0
23907	20150117	2200	20150117	1600	2.423	-98.08	30.62	18.4	18.6	19.0	18.4	0.0
23907	20150117	2300	20150117	1700	2.423	-98.08	30.62	17.8	18.2	18.5	17.8	0.0
23907	20150118	0000	20150117	1800	2.423	-98.08	30.62	16.2	16.9	17.8	16.2	0.0
23907	20150118	0100	20150117	1900	2.423	-98.08	30.62	15.9	16.2	16.4	15.9	0.0
23907	20150118	0200	20150117	2000	2.423	-98.08	30.62	14.8	15.2	15.9	14.8	0.0
23907	20150118	0300	20150117	2100	2.423	-98.08	30.62	14.4	14.6	14.9	14.3	0.0
23907	20150118	0400	20150117	2200	2.423	-98.08	30.62	13.7	13.8	14.4	13.7	0.0
23907	20150118	0500	20150117	2300	2.423	-98.08	30.62	13.4	13.5	13.7	13.3	0.0
23907	20150118	0600	20150118	0000	2.423	-98.08	30.62	12.4	12.9	13.5	12.4	0.0
23907	20150118	0700	20150118	0100	2.423	-98.08	30.62	12.2	12.1	12.3	11.9	0.0
23907	20150118	0800	20150118	0200	2.423	-98.08	30.62	11.1	11.6	12.2	11.1	0.0
23907	20150118	0900	20150118	0300	2.423	-98.08	30.62	10.4	10.7	11.1	10.4	0.0
23907	20150118	1000	20150118	0400	2.423	-98.08	30.62	9.8	10.2	10.6	9.8	0.0
23907	20150118	1100	20150118	0500	2.423	-98.08	30.62	9.6	9.7	9.9	9.4	0.0
23907	20150118	1200	20150118	0600	2.423	-98.08	30.62	8.7	9.2	9.6	8.7	0.0
23907	20150118	1300	20150118	0700	2.423	-98.08	30.62	8.6	8.6	8.8	8.2	0.0
23907	20150118	1400	20150118	0800	2.423	-98.08	30.62	8.2	8.7	9.5	8.2	0.0
23907	20150118	1500	20150118	0900	2.423	-98.08	30.62	11.6	9.8	11.6	7.6	0.0
23907	20150118	1600	20150118	1000	2.423	-98.08	30.62	15.6	13.6	15.6	11.6	0.0
23907	20150118	1700	20150118	1100	2.423	-98.08	30.62	16.9	15.9	16.9	15.0	0.0
23907	20150118	1800	20150118	1200	2.423	-98.08	30.62	17.8	17.0	17.9	16.2	0.0
23907	20150118	1900	20150118	1300	2.423	-98.08	30.62	18.5	18.0	18.6	17.4	0.0
23907	20150118	2000	20150118	1400	2.423	-98.08	30.62	19.9	19.2	19.9	18.4	0.0
23907	20150118	2100	20150118	1500	2.423	-98.08	30.62	20.2	19.9	20.4	19.3	0.0
23907	20150118	2200	20150118	1600	2.423	-98.08	30.62	20.8	20.5	20.8	19.7	0.0
23907	20150118	2300	20150118	1700	2.423	-98.08	30.62	19.3	20.1	20.9	19.3	0.0
23907	20150119	0000	20150118	1800	2.423	-98.08	30.62	16.5	17.9	19.3	16.4	0.0
23907	20150119	0100	20150118	1900	2.423	-98.08	30.62	15.0	15.5	16.5	15.0	0.0

Fig. E. Raw hourly data in Austin, TX (NOAA, 2015)

- 1^{st} column: the identification number of the observation site
- 4^{th} column: the local standard time date of the observation.
- 5^{th} column: the local standard time hour of the observation.
- 12^{th} column: the minimum air temperature in °C during the hour.

Appendix F

Hourly flight paths under Uncertainty Set 3

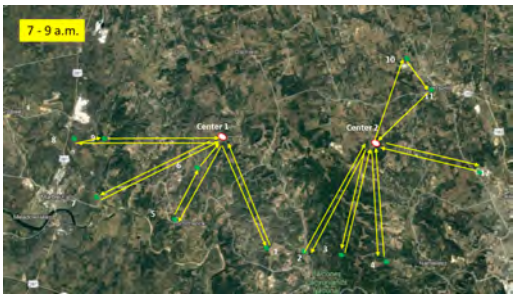

(a) From 7 a.m. to 9 a.m.

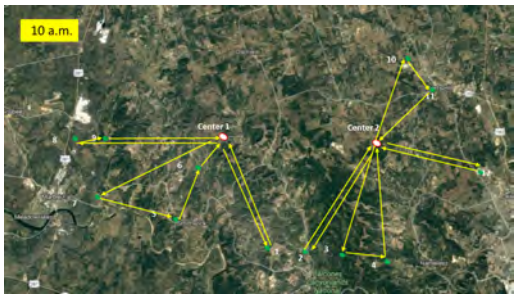

(b) At 10 a.m.

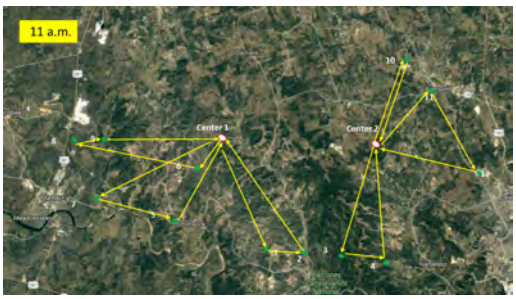

(c) At 11 a.m.

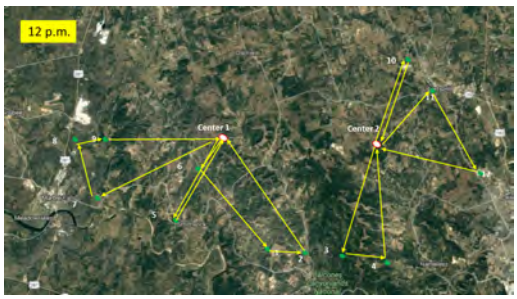

(d) At 12 p.m.

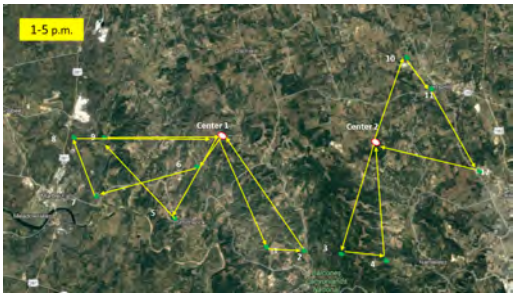

(e) From 1 p.m. to 5 p.m.

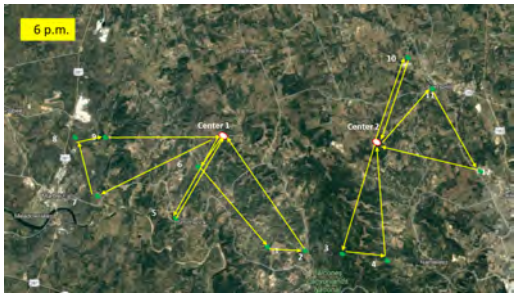

(f) At 6 p.m.

Fig. F. Hourly flight paths under Uncertainty Set 3

References

Al-Sabban, W. H., Gonzalez, L. F., Smith, R. N., 2013. Wind-energy based path planning for unmanned aerial vehicles using markov decision processes. In: Robotics and Automation (ICRA), 2013 IEEE International Conference on. IEEE, pp. 784–789.

Bazaraa, M. S., Jarvis, J. J., Sherali, H. D., 2011. Linear programming and network flows. John Wiley & Sons.

Bellvert, J., Zarco-Tejada, P. J., Girona, J., Fereres, E., 2014. Mapping crop water stress index in a pinot-noirvineyard: comparing ground measurements with thermal remote sensing imagery from an unmanned aerial vehicle. Precision Agriculture 15 (4), 361–376.

Ben-Tal, A., Nemirovski, A., 2000. Robust solutions of linear programming problems contaminated with uncertain data. Mathematical Programming 88 (3), 411–424.

Benham, J., 2015. Using Drones for Construction, Architecture, Engineering and Surveying. `http://jamesbenham.com` (Last accessed on June 21, 2016).

Bertsimas, D., Brown, D. B., Caramanis, C., 2011. Theory and applications of robust optimization. SIAM Review 53 (3), 464–501.

Bertsimas, D., Sim, M., 2004. The price of robustness. Operations Research 52 (1), 35–53.

Cho, J., Lim, G., Biobaku, T., Kim, S. J., Parsaei, H., 2015. Safety and security management with unmanned aerial vehicle (UAV) in oil and gas industry. Procedia Manufacturing 3, 1343–1349.

Daly, J., 2015. Disaster Relief Tech Goes All Out in Nepal. `http://www.wired.com` (Last accessed on June 21, 2016).

Deng, C., Wang, S., Huang, Z., Tan, Z., Liu, J., 2014. Unmanned aerial vehicles for power line inspection: A cooperative way in platforms and communications. Journal of Communications 9 (9).

d'Oleire Oltmanns, S., Marzolff, I., Peter, K. D., Ries, J. B., 2012. Unmanned aerial vehicle (UAV) for monitoring soil erosion in morocco. Remote Sensing 4 (11), 3390–3416.

FAA, 2016. FAA Doubles "Blanket" Altitude for Many UAS Flights. https://www.faa.gov/news/updates/?newsId=85264 (Last accessed on Aug 26, 2016).

GAMS Development, C., 2015. General Algebraic Modeling System (GAMS) Release 24.5.6. Washington, DC, USA, http://www.gams.com/.

Gordon, G., Tibshirani, R., 2012. Karush-kuhn-tucker conditions. Optimization 10 (725/36), 725.

Gorissen, B. L., Yanıkoğlu, İ., den Hertog, D., 2015. A practical guide to robust optimization. Omega 53, 124–137.

Hsu, J., 2013. Rise of the Drones: Unmanned Aircraft Sneak Into the Arctic. http://www.livescience.com/39194-drones-monitor-arctic.html (Last accessed on June 21, 2016).

IBM, 2015. CPLEX Optimizer. http://www.ibm.com/.

Kattel, D., Yao, T., Yang, K., Tian, L., Yang, G., Joswiak, D., 2013. Temperature lapse rate in complex mountain terrain on the southern slope of the central himalayas. Theoretical and applied climatology 113 (3-4), 671–682.

Kim, S. J., Lim, G. J., 2018. Drone-aided border surveillance with an electrification line battery charging system. Journal of Intelligent & Robotic Systems, 1–14.

Kim, S. J., Lim, G. J., Cho, J., Côté, M. J., 2017. Drone-aided healthcare services for patients with chronic diseases in rural areas. Journal of Intelligent & Robotic Systems 88 (1), 163–180.

Kunreuther, H., Heal, G., Allen, M., Edenhofer, O., Field, C. B., Yohe, G., 2013. Risk management and climate change. Nature Climate Change 3 (5), 447–450.

Langelaan, J. W., Alley, N., Neidhoefer, J., 2011. Wind field estimation for small unmanned aerial vehicles. Journal of Guidance, Control, and Dynamics 34 (4), 1016–1030.

Leng, F., Tan, C. M., Pecht, M., 2015. Effect of temperature on the aging rate of Li ion battery operating above room temperature. Scientific Reports 5.

Li, Z., Tang, Q., Floudas, C. A., 2012. A comparative theoretical and computational study on robust counterpart optimization: II. probabilistic guarantees on constraint satisfaction. Industrial & Engineering Chemistry Research 51 (19), 6769–6788.

Lim, G. J., Kim, S. J., Cho, J., Gong, Y., Khodaei, A., 2016. Multi-UAV pre-positioning and routing for power network damage assessment. IEEE Transactions on Smart Grid.

Lu, L., Han, X., Li, J., Hua, J., Ouyang, M., 2013. A review on the key issues for lithium-ion battery management in electric vehicles. Journal of Power Sources 226, 272–288.

McGonigle, A., Aiuppa, A., Giudice, G., Tamburello, G., Hodson, A., Gurrieri, S., 2008. Unmanned aerial vehicle measurements of volcanic carbon dioxide fluxes. Geophysical Research Letters 35 (6).

Merino, L., Caballero, F., Martínez-de Dios, J., Ollero, A., 2005. Cooperative fire detection using unmanned aerial vehicles. In: Proceedings of the 2005 IEEE international conference on robotics and automation. IEEE, pp. 1884–1889.

Miller, C. E., Tucker, A. W., Zemlin, R. A., 1960. Integer programming formulation of traveling salesman problems. Journal of the ACM (JACM) 7 (4), 326–329.

Nichols, C. P., 2014. Drones: The coming of age of a not-so-new technology. Judges J. 53, 20.

NOAA, 2015. Hourly Dataset in Austin, TX. `http://www1.ncdc.noaa.gov/pub/data/uscrn/` (Last accessed on Feb 29, 2016).

Öncan, T., Altınel, İ. K., Laporte, G., 2009. A comparative analysis of several asymmetric traveling salesman problem formulations. Computers & Operations Research 36 (3), 637–654.

Rao, R., Vrudhula, S., Rakhmatov, D. N., 2003. Battery modeling for energy aware system design. Computer 36 (12), 77–87.

Stolaroff, J., 2014. The need for a life cycle assessment of drone-based commercial package delivery. Tech. rep., Lawrence Livermore National Laboratory (LLNL), Livermore, CA.

Tech, P., 2016. Discharge curve at different temperature-EN. http://www.powertechsystems.eu/g2-en/ (Last accessed on June 21, 2016).

Torres-Sánchez, J., López-Granados, F., De Castro, A. I., Peña-Barragán, J. M., 2013. Configuration and specifications of an unmanned aerial vehicle (UAV) for early site specific weed management. PLoS One 8 (3), e58210.